nuclear fusion
IAEA

PAPER • OPEN ACCESS

Generation of energetic electrons during X2 ECRH start up

To cite this article: C. Albert Johansson *et al* 2025 *Nucl. Fusion* **65** 056009

OPEN ACCESS
IOP Publishing | International Atomic Energy Agency
Nuclear Fusion
Nucl. Fusion **65** (2025) 056009 (8pp)
https://doi.org/10.1088/1741-4326/adc1de

Generation of energetic electrons during X2 ECRH start up

C. Albert Johansson*, Pavel Aleynikov, Per Helander, Dmitry Moseev and the W7-X team[a]

Max-Planck Institute for Plasma Physics, Wendelsteinstraße 1, 17491 Greifswald, Germany

E-mail: albert.johansson@ipp.mpg.de

Received 13 November 2024, revised 10 February 2025
Accepted for publication 18 March 2025
Published 2 April 2025

Abstract

In the initial stages of plasma initiation in the Wendelstein7-X stellarator with electron-cyclotron-resonance heating, a downshifted electron cyclotron emission signal is observed. Due to the absence of a corresponding upshifted signal, this signal is believed to come from energetic electrons (∼10 keV). We propose a mechanism for the generation of these fast electron based on the overlap of cyclotron resonances on flux surfaces close to the centre of the plasma. Multiple passages through these resonances lead to the stochastisation of particle trajectories, which ultimately results in the formation of a quasi-steady-state electron distribution function that is predominantly flat in energy space across regions of resonance overlap. The electron cyclotron emission of such a distribution function agrees with the experimental observations.

Keywords: electron cyclotron resonance, ECR, ECRH, electron cyclotron emission, ECE, supra-thermal electrons, start-up

(Some figures may appear in colour only in the online journal)

1. Introduction

During the initial stages of plasma formation with electron cyclotron resonance heating (ECRH) in Wendelstein 7-X (W7-X), electron-cyclotron-emission (ECE) measurements reveal the presence of suprathermal electrons. The evidence is derived from the observation of a low-frequency ECE spectrum that does not show a corresponding increase at higher frequencies. The downshifted frequency of the emission corresponds to electrons located close to the magnetic axis with energies ranging from 5 to 50 keV, with a main peak corresponding to electrons at around 10 keV. These observations are puzzling since the plasma temperature is believed to be far lower at this stage of the discharge. The presence of energetic electrons during ECRH operation has also been observed in the Wendelstein 7-A [1] and TJ-II [2] stellarators.

ECRH utilises high-power electromagnetic waves in the millimetre-wave range [3, 4]. The interaction between the waves and particles is nonlinear during the startup phase, allowing cold electrons to be accelerated to relatively high energies in a single pass through the ECRH beam [5, 6]. The mean free path of such electrons is much longer than the size of the machine, so they can be considered to be predominantly collisionless. Under the conditions of W7-X, these single-pass energy gains result in electrons with energies up to 1 keV, which is however insufficient to account for the observed downshifted ECE signals. Therefore, multiple resonant interactions are necessary for the generation of particles with energies around 10 keV.

The electron trajectories in phase space can be described by a time-independent Hamiltonian [6–9], whose conservation imposes a limit on the total energy gain. This gain is effectively constrained by the relativistic resonance width. Due to this

[a] See Grulke *et al* 2024 (https://doi.org/10.1088/1741-4326/ad2f4d) for the W7-X Team.
* Authors to whom any correspondence should be addressed.

restriction, even if an electron traverses the same resonance location multiple times, its energy cannot increase beyond a certain limit, since neither the resonance width nor the central resonant frequency change. Consequently, a change in resonance condition is required for gaining energies significantly higher than 1 keV, making the observation of 10 keV electrons puzzling.

We suggest that the generation of fast electrons in W7-X may be attributed to a multi-step process, which can be understood as follows. Suppose that an electron traveling along the magnetic field passes through the ECRH beam once and gains some energy due to the resonant interaction. Whether an electron can efficiently gain energy is governed by the resonance condition,

$$n\frac{\omega_c}{\gamma} + v_\parallel k_\parallel - \omega = 0, \tag{1}$$

where ω is the wave angular frequency, $\omega_c = eB/m$ the non-relativistic cyclotron frequency, B the magnetic field strength, e the elementary charge, m the rest mass, $\gamma \equiv \sqrt{1+\boldsymbol{p}^2/(m^2c^2)}$ the Lorentz factor, and $\boldsymbol{p} = \gamma m\boldsymbol{v}$ the relativistic momentum. The quantities $v_\parallel$ and $k_\parallel$ denote the particle's parallel velocity and the wave vector parallel to the magnetic field, respectively, and n is an integer corresponding to the resonance harmonic.

Since the electron has gained energy, the resonance condition with the same wave frequency ω is now satisfied at a higher ω_c, i.e. at a higher magnetic field strength B. Therefore, this particle may only gain energy again if, the next time it crosses the ECRH beam, it does so in a region of higher magnetic field strength B. By repeatedly changing the magnetic field strength between interactions, the electron in question experiences random jumps in velocity space. Because of the change in the resonant condition, the particle may gain energies much larger than those through a linear or nonlinear interaction in a single passage through the beam or by passing through the beam repeatedly at constant field strength.

Indeed, it follows from equation (1) that a change in the magnetic field strength of 0.2% yields a shift in the resonant energy by approximately 1 keV, since

$$mc^2\delta\gamma = mc^2\frac{\delta B}{B}, \tag{2}$$

excluding the Doppler shift[1]. An electron that has already gained this amount of energy through a single interaction with an ECRH beam can gain an additional 1 keV if its trajectory takes it to another region of the beam where the magnetic field strength is 0.2% higher. In the W7-X stellarator, a magnetic field variation of 0.2% corresponds to a radial shift of about 0.5 cm. This distance is smaller than the ECRH beam radius, which is about 4 cm, implying that flux surfaces close to the magnetic axis are entirely enveloped by the beam but that any particle interacting with the beam quickly moves out of resonance.

[1] If $k_\parallel c/\omega \approx 0.1$, then $v_\parallel$ must change by $0.1c$ (i.e. 5 keV) to obtain as large of an effect as a 1 % change in the magnetic field. The beams are typically aimed such that $k_\parallel c/\omega \ll 0.1$.

2. Resonance overlap due to rotational transform

Thanks to the complexity of charged-particle motion in toroidal magnetic fields, there are several possibilities for an electron to interact with the same ECRH beam at different locations (with varying magnetic field strengths). For example, Neishtadt [8] considered the drift of adiabatically trapped electrons and found that a halo of fast particles can be created. Zvonkov [10] paired this change in resonance condition with the bounce motion, which imposes an upper bound on the energy gain. In a stellarator, trapped particles can drift across flux surfaces; however, due to magnetic moment conservation, they cannot move to regions of higher magnetic field strength than their bounce points.

Moreover, in W7-X experiments, the beams are usually aimed at a toroidal position close to the maximum magnetic field strength on axis. Therefore, most of the accelerated electrons are expected to be passing (rather than magnetically trapped) and thus experience very little net radial drift. Instead, passing electrons traverse the torus, and their poloidal angle change by the rotational transform ι times $\pm 2\pi$ for each turn around the torus. After travelling any number of times around the torus, such particles again intersect the ECRH beam, but at a poloidal position with different magnetic field strength. If this strength is matched to the energy reached in the previous passage through the beam, resonant interaction becomes possible again, thus enabling additional energy gain. If subsequent interactions occurring in this way exhibit resonance overlap, the energy can grow substantially.

The width in energy of the resonance around the resonance condition can be calculated approximately using [6, 9]

$$W \approx mc^2\frac{\sqrt{\frac{E_- N_\perp}{cB}\left(1+\frac{N_\parallel p_\parallel}{mc}-\frac{m\omega}{neB}-\frac{p_\parallel^2}{2m^2c^2}\right)}}{1-N_\parallel^2}, \tag{3}$$

where E_- is the magnitude of the electric field rotating in the electron direction, and $N_\perp$ is the wave refractive index orthogonal to $\boldsymbol{B}$. This width describes nonlinear resonant wave-particle interaction, in which the electrons follow a pendulum-like phase-space structure in the action variable $\frac{m}{e}\mu$ with characteristic width given by equation (3). The fractional energy gain for low-energy particles cannot be considered as small, as typically assumed in standard quasi-linear theory.

We now illustrate the resonance overlap mechanism with a quantitative analysis, considering the W7-X standard magnetic configuration, dubbed 'EIM' in W7-X nomenclature. Flux surfaces near three of the ECRH beams (in blue) are depicted with solid lines in both figures of figure 1.

Resonance overlap is guaranteed on an irrational flux surface covered by the beam. However, in this configuration $\frac{7}{6}\iota \approx 1$ to within 0.3 % near the magnetic axis, which represents a more restrictive case of an almost rational flux surface, where the particle interacts with the wave at a discrete number of different poloidal locations before returning to its starting point. The corresponding resonances must therefore have a sufficiently large width to ensure the overlap. The case of rational

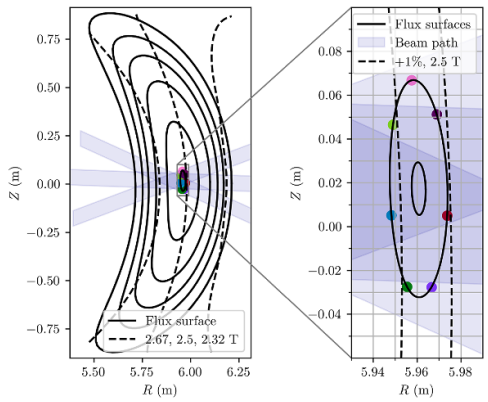

Figure 1. Magnetic field geometry at gyrotron aiming position for W7-X standard configuration. 7 points are marked, each with a poloidal angle shifted by $2\pi\,\iota$ from the other.

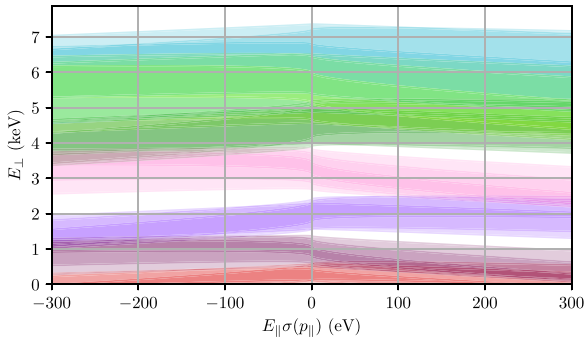

Figure 2. Resonance regions of the beams at the different beam intersection points. An electron located near the pink position in figure 1 is simultaneously influenced by three waves. Each wave, on its own, creates a separatrix, the maximum extent of which spans the area marked in pink here. The other colours similarly refer to the correspondingly coloured positions in figure 1. Here, $E_\perp = \frac{p_\perp^2}{2m}$ is the non-relativistic energy perpendicular to $\boldsymbol{B}$, $E_\parallel$ the parallel energy, and σ denotes the sign of $p_\parallel$.

flux surface is qualitatively similar to the general case but less costly computationally, since it allows us to employ a pre-computed map of the wave-particle interactions. In our case the electrons will remain near seven intersection points with poloidal angles given by $\theta_i = \theta_j + 2\pi\,(i-j)\iota(\psi)$ (see figure 1). These points are located at the flux surface $\psi = 0.0026\psi_{\max}$, where $\psi_{\max} = 1.95$ Wb denotes the toroidal magnetic flux through the last closed flux surface.

Figure 2 shows the phase-space structure at these points in terms of the resonance width equation (3) indicated by colours corresponding to the positions displayed in figure 1. That is, an electron located at the peak of the wave-field intensity, with an energy corresponding to the colour of this spatial point, will be inside the wave-particle separatrix. The colour coding corresponds to that of the points in figure 1. There is one resonance region for each of the three different beams at each point. When two resonances overlap we can expect from the Chirikov criterion that electrons will have chaotic orbits [11]. Over many bounces/torus passes, electrons will explore the phase space covered by all these resonances. We therefore expect the formation of a *flat distribution function*, provided that electrons can become passing (either generated as passing or through scattering). This distribution will be uniformly distributed in energy up to the highest resonant one, which is approximately 7 keV in this case. In the next section, we use numerical modelling to validate this illustrative picture.

3. Calculation of the distribution function

A more accurate prediction of the distribution function can be obtained from the equations of motion (EOM), equation (2.23) in [6]. These equations have been solved numerically within the ECRH beam to obtain a map $(\Theta, \mu, p_\parallel) \mapsto (\gamma)$ for each of the seven intersection points, where Θ is the gyro-angle and $\mu = \frac{p_\perp^2}{2mB}$ is the magnetic moment. This map takes the electrons initial values before the beam interaction and maps them to the exit particle energy, and correctly takes care of the parallel wave-vector. The numerical solution of the EOM correctly captures both the linear and nonlinear regimes of the wave-particle interaction.

Because particles primarily gain perpendicular energy from the wave and the interaction occurs near the magnetic axis, it is expected that most of them will be near the trapped-passing boundary or within the trapped region, which would prevent further energy gain since magnetically trapped particles bounce back and forth along the same field line and encounter the resonance at the same field strength every time. However, the particles also undergo collisions, which, although weak, can detrap particles and enable larger energy gains. We model collisional scattering of our suprathermal electrons outside the beam using a Monte Carlo approach, similar to references [12, 13]. The large energy gained in one beam passage ensures that the collisions are weak. The bounce-averaged equations for the momentum and the pitch angle evolution are

$$\Delta\lambda = 2\nu_D \left(\frac{\zeta_2}{\zeta_1} - \frac{\lambda}{2}\right)\Delta t + \sqrt{2\nu_D \lambda \frac{\zeta_2}{\zeta_1}}\,\xi\,\sqrt{\Delta t} \tag{4}$$

$$\Delta p = -\nu_p p \Delta t \tag{5}$$

where $\xi \sim \mathcal{N}(0,1)$ is a normal (0,1) random variable and $\lambda \equiv 2m\mu B_{\max}/p^2$. Momentum diffusion can be ignored since the velocity of the colliding particles is much higher than the thermal velocity of the species they collide with. In our case, collisions are dominated by interactions with neutral hydrogen; the corresponding scattering frequency is [14]

$$\nu_D = \frac{me^4 n_{\mathrm{H}}}{4\pi\epsilon_0^2} \frac{\sqrt{1+\frac{p^2}{m^2c^2}}}{p^3}\left[2.5632 + \ln\left(\frac{p}{13\alpha mc}\right)\right], \tag{6}$$

where $\alpha \simeq 1/137$ is the fine-structure constant, n_{H} the neutral hydrogen density, and the corresponding slowing down frequency is given by the Bethe slowing down formula [14]

$$\frac{p}{m\gamma}\frac{\mathrm{d}p}{\mathrm{d}t} = \frac{\mathrm{d}E}{\mathrm{d}t} = -\frac{e^4 n_\mathrm{H}}{8\pi\epsilon_0^2 m v}\left[\ln\frac{c^2p^2(\gamma-1)}{2I^2} - \left(\frac{2}{\gamma}-\frac{1}{\gamma^2}\right)\ln(2) + \frac{1}{\gamma^2} + \frac{(\gamma-1)^2}{8\gamma^2}\right] \equiv -\frac{\nu_p p^2}{m\gamma}, \tag{7}$$

where $I \approx 18.2\,\mathrm{eV}$ for hydrogen [15].

Two integral coefficients ζ_1 and ζ_2 in equation (4) arise from the bounce averaging. The variation of the magnetic field strength along the trajectory in the W7-X standard configuration can be adequately represented for the purpose of bounce averaging with a simple $\cos(\hat{l})$ dependence, where $\hat{l}$ is a field-line-following coordinate. This yields

$$\zeta_1 = \oint \frac{1}{2\pi\sqrt{1-b\lambda}}\mathrm{d}\hat{l} = \frac{4}{\pi\sqrt{1+(2B_1-1)\lambda}}\Re\left(K(\kappa)\right) \tag{8}$$

$$\zeta_2 = \oint \frac{\sqrt{1-b\lambda}}{2\pi}\mathrm{d}\hat{l} = 4\frac{\sqrt{1+(2B_1-1)\lambda}}{\pi}\Re\left(E(\kappa)\right) \tag{9}$$

with the following definitions

$$b = 1 - B_1 - B_1\cos\left(\hat{l}\right), \tag{10}$$

$$\kappa \equiv \frac{2B_1\lambda}{2B_1\lambda-\lambda+1}, \tag{11}$$

$$B_1 \equiv \frac{B_\mathrm{max}(s) - B_\mathrm{min}(s)}{2B_\mathrm{max}} \tag{12}$$

and $\Re$ denotes the real part. Within this model, the ratio ζ_2/ζ_1, which appears in the equation of motion (4) and (5), is independent of the number of modules travelled by the particle before the bounce. The functions K and E are complete elliptic integrals of the parameter κ of the first and second kinds, respectively. Note that equation (15c) in [12] contains a typo where ζ_1/ζ_2 should be replaced with ζ_2/ζ_1.

The combined procedure for the calculation of the distribution function is as follows. First, the energy gain from the beams is calculated using linear interpolation of the map obtained from the numerical solutions of the EOM (2.23) from [6] assuming that the initial phase Θ is a uniformly distributed random variable. The magnetic moment is then calculated using the conserved wave-particle Hamiltonian [6, 8, 9, 16]

$$H = mc^2\gamma - \frac{\omega}{n}\frac{m}{e}\mu. \tag{13}$$

Second, we verify that the particles with updated γ and μ can reach the next interaction point after leaving the beam. If they bounce, they return to the same interaction location with a reversed sign of $p_\parallel$. The electrons that do not bounce interact with the beams at the next position according to the rotational transform. The value of $p_\parallel$ is updated by conserving energy and μ. For this step we use the exact W7-X magnetic configuration.

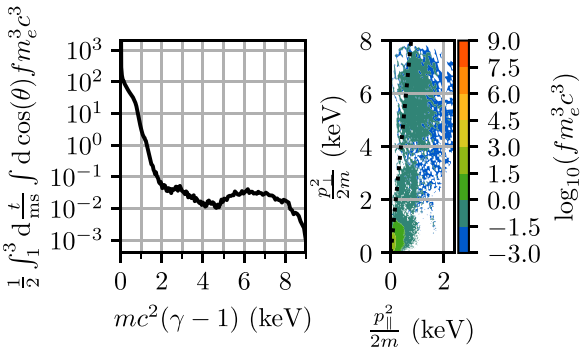

Figure 3. Distribution function averaged over the times 1 ms to 3 ms to increase statistical significance. Left: pitch angle averaged distribution function, right: 2D distribution function where the λ and μ are transformed to perpendicular momentum, $p_\perp$, and parallel momentum, $p_\parallel$, at the minimum magnetic field on the considered flux surface.

Finally, we account for the effect of collisions by applying equations (4) and (5) with Δt equal to the bounce time

$$t_b \approx N\frac{R_\mathrm{W7X}}{5v}\zeta_1, \tag{14}$$

where $R_\mathrm{W7X} = 6\,\mathrm{m}$ is approximately the machine radius. For trapped particles N is equal to the number of modules traversed between two bounces, while for passing electrons $N = 5$. The value of N ranges from 1 to 5 due to the fact that the magnetic field in W7-X is such that some electrons reside in trapping wells that extend over several periods of the device. Collisions with other particles can cause passing electrons to become trapped, or vice versa, thus randomising the sign of $p_\parallel$. Low-energy electrons undergo multiple collisions over the course of traversing the torus, in contrast to the energised electrons, whose collision time is significantly longer. In the event that the bounce time exceeds the collision time, the electron is re-initialised with a 10 eV Maxwell–Boltzmann distribution.

Eight thousand particles were simulated for 9 ms. These were initiated with a Maxwell-Boltzmann distribution of 10 eV, a representative energy for secondary electrons. The distribution function evolves continuously, but reaches a quasi-steady state after about 0.5 ms. A slow expansion of the distribution function into high energies is observed. This is connected with the slow increase of the $p_\parallel$. However on the timescale of interest the distribution function is found to change very slowly. The maximum obtained energy after 9 ms is around 10 keV.

The distribution function is shown in figure 3, where two distinct regions can be identified. The first region is roughly between 0 and 2 keV, where the distribution function decreases rapidly with increasing energy. The second region is located between 2 and 8 keV, the distribution function is almost flat due to resonance overlap. The distribution function is flat up to the maximum overlap because the diffusion of particles due to pitch angle scattering allows for deviation from the Hamiltonian contours, ultimately extending the resonant interaction in energy.

The 2D-distribution function is shown in the right panel of figure 3 as a function of the parallel and perpendicular momenta at the location of minimum magnetic field, $B_{\min}$. The trapped-passing boundary is indicated by a dotted line. As evident from the figure, the high-energy tail of the distribution is anisotropic due to the heating, which preferentially increases the perpendicular momentum. The electrons in the tail have, however, also gained parallel momentum in comparison with the thermal population, which occurs for two different reasons. Pitch-angle scattering transfers energy from the perpendicular to the parallel direction, and the mirror force has a similar effect on particles travelling from the resonance location to that of the minimum magnetic field, $B_{\min}$.

4. Comparison with experimental data from W7-X

W7-X is a stellarator with five field periods (modules) that uses superconducting coils to produce the magnetic field. The latter possesses good flux surfaces and is accurate to one part in 100 000 [17].

To achieve breakdown, ECRH is typically used with X2-mode polarisation at a frequency of 140 GHz [4], which is twice the electron cyclotron frequency at the nominal field of 2.5 T. In the experiments under consideration, the microwave system consisted of 10 gyrotrons, each capable of delivering 1 MW, although only up to 8 MW passes through the ports. However, the gyrotrons were detuned to 6 MW port-through power to avoid arcing in the transmission lines. Each gyrotron beam can be steered via a mirror to achieve on-axis or off-axis heating, in either O-mode or X-mode, and is delivered as a Gaussian wave with a beam width of 4 cm. We focus on experiments with on-axis heating using the X2 mode.

In a module without ECRH ports, a 32-channel radiometer, set up in X2-mode polarisation with a frequency band close to 140 GHz, is used to measure the ECE emission [18–20]. The measured emission angular frequency is thus equal to

$$\omega = 2\frac{\omega_c}{\gamma} + v_{\parallel}k_{\parallel}, \tag{15}$$

and the position of the port is such that $k_{\parallel}$ is very small. Somewhat surprisingly, at the very beginning of many discharges, a downshifted ECE spectrum is observed compared to the expected one from a plasma located close to the magnetic axis. We propose that this is the result of a combined effect of the generation of fast (multi-keV) electrons and their radial transport, which is expected to be neoclassical at this stage in the discharge history. The mechanism is discussed in full detail in section 5.

Although many experiments at W7-X show a downshifted ECE signal, we apply the following criteria to select experiments and narrow down the cause of the downshift:

- For simplicity, as few gyrotrons as possible, and no other heating systems, should be active, which in these experiments means that four ECRH beams are operative.
- The heating power should be absorbed close to the magnetic axis.

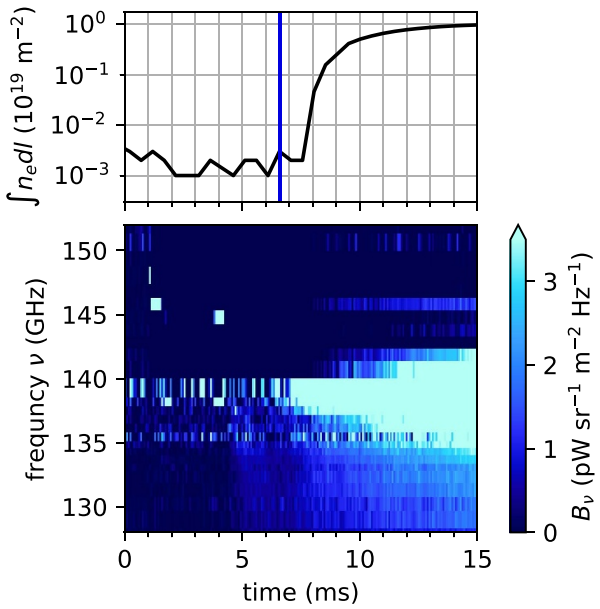

Figure 4. Line integrated density top graph and spectral radiance from experiment 20221129.36. The time of the spectrum in figure 5 is shown with a vertical line.

- We only consider discharges using one particular magnetic configuration.

These criteria narrowed down the list to discharges #20221130.31, #20221129.36, and their repeats, which used gyrotrons C1, D1, E1, and B5 (in W7-X nomenclature). Experiments also exist involving C1, D1, E1, and A5, but these yielded two additional peaks in the ECE spectrum, both shifted by 5 GHz from the central 140 GHz frequency—one downshifted and one upshifted. Otherwise the spectra were similar, but these discharges were nevertheless excluded from our analysis, since the shifted peaks could, in principle, have resulted from off-axis heating.

Figure 4 shows the evolution of the line-integrated density measured with the interferometer [21], and the ECE spectrogram [18–20] from the discharge #20221129.36. The gyrotrons were turned on at $t = 0$, and the ECE spectrum given by the spectral radiance is shown in the bottom plot, where we note that a pronounced tail extends towards downshifted frequencies. As the plasma is believed to be created at the resonance condition (in this case, the magnetic axis), such a downshift would correspond to 10–50 keV electrons at the magnetic axis. The lack of an upshifted counterpart excludes the possibility of low-energy electrons being spread over the full flux-surface. At 6.3 ms, marked with a blue vertical line, a downshifted spectrum exists even though the line-integrated density is below the noise level of about 3×10^{16} m^{-2}. This line-integrated density is too low for low-energy electrons (from tens of eV to hundreds of eV) to cause the spectra, since a tail of such electrons would not produce the necessary intensity. Moreover, such electrons would have to be unevenly distributed over the flux surface to account for the lack of an upshifted emission counterpart. Therefore, we deduce the existence

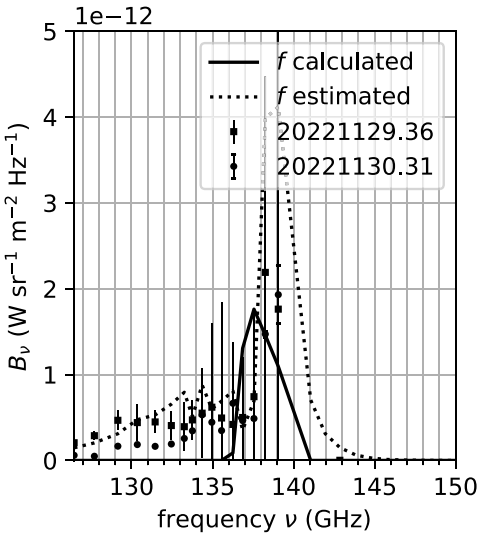

Figure 5. The measured spectra for different experiments are shown with squares and circles. The electron cyclotron emission spectrum of figure 3 with a black solid line. The spectrum from an estimated distribution function, which includes the effect of drifts, is shown with a dotted line.

of a suprathermal electron population. Unfortunately, their low density in combination with the short time-window available for detection prevent direct measurements of these fast electrons by other means.

Figure 5 shows experimental spectra, averaged over a time range of 0.4 and 0.1 ms, for W7-X discharges #20 20221129.36 (discussed above) as well as #20221130.31, in squares and circles with caps, respectively. The displayed error represents the sum of the statistical variances associated with the respective data-points' contribution to the time-averaged value. Additionally, a ray tracing calculation using the TRAVIS code [22] of the ECE spectrum resulting from the distribution function shown in figure 3 is shown by a solid black line. TRAVIS uses conventional ray tracing and solves the radiation transport equation (which includes the parallel wave-vector), accounting for both re-absorption and emission to calculate the spectra. Although the absorption of the strong ECRH beam is highly nonlinear, the emission of a weak ECE signal is still described by conventional linear theory. The calculated re-absorption is less than 10.2 %. The spectral intensity is set by the electron density, which has been assumed to be constant in the centre of the plasma, $s < 0.0026$. We choose this density to be $n_e = 6 \times 10^{18}\,\mathrm{m}^{-3}$, so that the intensity is similar to the measured one. It is important to note that most electrons are relatively cold and do not contribute much to the measured ECE signal. The density of electrons with energies above 2 keV is around $5.8 \times 10^{15}\,\mathrm{m}^{-3}$.' to 'slow' electrons is thus about 1 to 1000, confirming the conjecture that the typical electron energy is much lower than several keV. This assumed density is not in contradiction with the measured line-integrated density, because its spread is only a few centimetres.

The experimentally measured spectra (discharge #20221129.36 and #20221130.31) and the calculated spectra are in good agreement in the mid-range frequencies (137−142 GHz). However, the proposed energetic-particle distribution function (capped close to 10 keV by the structure of the resonances) cannot explain the lower-frequency (<137 GHz) spectra observed experimentally.

We note a considerable discrepancy between the modelled and observed spectrum in the low-frequency range (<137 GHz). This low-frequency signal extends to the lowest channel at 126 GHz, corresponding to the presence of 50 keV electrons in the proximity of the magnetic axis. Generation of such electrons is precluded by the resonance picture given in figure 2. These electrons must therefore be located at outer flux surfaces and probably originate from magnetically trapped electrons that have drifted radially. Indeed a significant fraction of up to 16 % of the electrons observed in our modelling are trapped. We will consider drifts to outer flux surfaces and estimate the distribution function leading to the dotted line in figure 5.

5. Radial drift of energetic electrons

In the absence of collisions, magnetically trapped electrons follow orbits of constant second adiabatic invariant [23, 24]

$$J(B_b(\lambda), s, \alpha) = \oint v_\parallel \mathrm{d}\hat{l} = \sqrt{\frac{2E}{m}} \oint \sqrt{1 - \frac{B\left(\hat{l}\right)}{B_b}}\,\mathrm{d}\hat{l}, \quad (16)$$

where α is the Clebsh-angle [24]. W7-X has been shown to produce a very accurate magnetic field configuration [17], such that these orbits are realised. Figure 6 shows the contours of this quantity, where B_b is the magnetic field strength at the bounce points. The contours are shown for the standard W7-X configuration which was used in the experiments discussed above. The bounce field is chosen to be $B_\mathrm{b} = 2.54$ T, 1.4 % above the resonant magnetic field. Only the trajectories which cross the toroidal angle of the ECE antenna are taken into account, i.e. the electrons trapped in the wells which do not contribute to the measured ECE signal are ignored. The line-of-sight for the ECE antenna is shown with a thick red line. Figure 6 demonstrates that there are no collisionless drift trajectories that connect regions close to the magnetic axis, $s < 0.0026$, (where the energetic electrons are generated) to where the lower-frequency ECE spectra could have been generated (i.e. along ECE line-of-sight at $\alpha \approx 8°$ for $s > 0.4$). The problem is that only trapped particles can drift across flux surfaces but their orbits are constrained from moving into regions where the ECE signal in question was produced. However, it seems quite possible that collisional scattering of such particles onto passing orbits could transport electrons to this region and thus explain the lower-frequency signal in the spectra.

In order to assess this mechanism, we note that the collision timescale given by equation (6) is of the order a few ms for

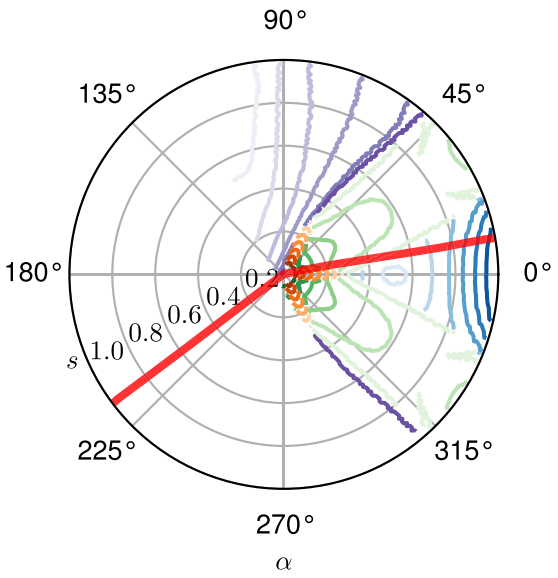

Figure 6. Drift orbits in purple, blue, green, and orange lines. Different colours represent bouncing in 1, 2, 3 or 4 modules respectively. Coordinate is field line label $\alpha = (\theta - \iota\varphi) \mod 2\pi$ and radius is flux surface label $s \equiv \psi/\psi_{\max}$. The ECE antenna line-of-sight is shown with a thick red line.

10 keV electrons, and so is the drift timescale [23]

$$\tau_d \approx \frac{e\psi_{\max} t_b}{\frac{\partial J}{\partial \alpha}}, \tag{17}$$

where

$$t_b(\mu, E, s, \alpha) = \oint \frac{\mathrm{d}\hat{l}}{v_\parallel} \tag{18}$$

denotes the bounce time. It follows that fast electrons will indeed drift radially and be collisionally scattered into the region where the ECE signal must have been produced, and that this will all occur on the timescale of the measurements.

For a quantitative estimate, we take the fast-electron distribution function to be given by

$$f(s,t,E,\lambda) \propto n(s,t)\,\Theta\left(E_{\mathrm{m}}(s) - E\right)\Theta \times \left(\lambda - \frac{6}{8}\frac{B_{\max}(s=0.0026)}{B_{\min}(s=0.0026)}\right), \tag{19}$$

where the Heaviside step function Θ ensures that the energy distribution is flat up to the maximum resonant energy $E_{\mathrm{m}}(s)$, which depends on the flux surface s. The pitch-angle distribution of the fast electrons in figure 3 is replicated by implementing a cutoff at the pitch-angle of the point represented by the coordinates $(p_\perp^2/2m, p_\parallel^2/2m) = (6\mathrm{keV}, 2\mathrm{keV})$. The density $n(s,t)$ of these fast electrons is taken to be approximately governed by the neoclassical transport equation,

$$\frac{\partial n}{\partial t} = \frac{D_{11}}{a^2}\frac{1}{\rho}\frac{\partial}{\partial \rho}\rho\frac{\partial n}{\partial \rho}, \tag{20}$$

where $a \approx 0.52\,\mathrm{m}$ is the minor radius of the last closed flux surface and $\rho = \sqrt{s}$. In reality, the diffusion coefficient D_{11} will differ somewhat from that of standard neoclassical theory due to the peculiar pitch-angle dependence of our distribution function, but we ignore this complication. $D_{11}/a^2 \approx 3.1\,\mathrm{Hz}$ for 10 keV electrons, as calculated in [25] at $\nu_* = 1.5 \times 10^{-5}$, consistently with the scattering given by equation (6). Using the distribution function obtained in this way, TRAVIS is once again employed to calculate the ECE spectrum, which is shown as a dotted line in figure 5. The boundary condition $n(s = 0.0026) = n_{nc0} = 5.8 \times 10^{15}\,\mathrm{m}^{-3}$ has been chosen in alignment with the fast particle density of the previous section. The emission intensity at approximately 140 GHz is higher due to the fact that the emission from energetic electrons on the high-field side occurs in close proximity to 140 GHz, irrespective of the flux surface. At the high-field side, the variation in magnetic field precisely aligns with the alteration in the Lorentz factor, γ, in accordance with the resonance condition. Therefore, no upshifted signal is observed, even though the density is a flux function. Conversely, on the low field side, the variation in B and the alteration in γ combine, and ~ 20 keV electrons are enough to explain the lowest observed frequency. It should be noted that the value of the boundary condition is arbitrary and therefore only the relative heights can be compared. Within the observational uncertainties, the measured spectrum is reproduced by this calculation. Calculation of the time evolution of the spectra would require modelling of the bulk-plasma ionisation processes; this is planned for future work.

6. Conclusions

In summary, energetic ($\sim$10 keV) electrons are indirectly observed during ECRH-induced plasma breakdown in the W7-X stellarator, which is puzzling since the electron temperature is believed to be much lower than this value. Moreover, an electron cannot gain more than about 1 keV when passing through the ECRH beam due to relativistic detuning of the cyclotron resonance, even if it were to travel through the same resonant location multiple times.

However, the observations become intelligible by realising that the magnetic geometry of the stellarator enables resonant wave-particle interaction to occur in several places on the same flux surface. Due to Chirikov overlap of these resonances, single electrons can thereby gain significant energy in the direction perpendicular to the magnetic field. This will tend to make them magnetically trapped and, as a consequence, drift to other flux surfaces. Upon collisional scattering, they can again become untrapped (passing), making them able to access the entire flux surface and thus move into regions of further resonant interaction. When this process is repeated, a random walk ensues and enables electrons to gain energies high enough to explain the observed ECE spectra on the relevant time scale. This qualitative picture is confirmed by numerical modelling, which, although approximate, is based on first principles and reproduces the measured spectrum without any free parameters other than a single scaling factor determining the overall amplitude of the signal.

Although we deduced that the downshifted ECE-spectrum originates from energetic electrons, it is not necessarily a unique solution. Specifically, for each particle energy, there is a density and magnetic field strength that yield a specific combination of emission-intensity and -frequency. However, a low-energy electron-distribution-function seems unlikely, because collisions should isotropise such a distribution function, yielding a spectrum almost symmetric around 140 GHz.

Acknowledgments

This work has been carried out within the framework of the EUROfusion Consortium, funded by the European Union via the Euratom Research and Training Programme (Grant Agreement No 101052200 - EUROfusion). Views and opinions expressed are however those of the author(s) only and do not necessarily reflect those of the European Union or the European Commission. Neither the European Union nor the European Commission can be held responsible for them.

ORCID iDs

C. Albert Johansson https://orcid.org/0000-0002-0956-9186
Pavel Aleynikov https://orcid.org/0009-0002-3037-3679
Per Helander https://orcid.org/0000-0002-0460-590X
Dmitry Moseev https://orcid.org/0000-0001-7955-8565

References

[1] Wilhelm R., Erckmann V., Janzen G., Kasparek W., Muller G., Rauchle E., Schuller P.G., Schworer K. and Thumm M. 1984 Electron cyclotron resonance heating and confinement in the W VII-A stellarator *Plasma Phys. Control. Fusion* **26** 1433
[2] Ochando M.A., Medina F., Zurro B., McCarthy K.J., Pedrosa M.A., Baciero A., Rapisarda D., Carmona J.M. and Jiménez D. 2006 Effect of suprathermal electrons on the impurity ionization state *Plasma Phys. Control. Fusion* **48** 1573
[3] Wolf R.C., Bozhenkov S., Dinklage A., Fuchert G., Kazakov Y.O., Laqua H.P., Marsen S., Marushchenko N.B., Stange T., Zanini M. and Abramovic I. 2018 Electron-cyclotron-resonance heating in Wendelstein 7-X: a versatile heating and current-drive method and a tool for in-depth physics studies *Plasma Phys. Control. Fusion* **61** 014037
[4] Laqua H.P. *et al* 2021 High-performance ECRH at W7-X: experience and perspectives *Nucl. Fusion* **61** 106005
[5] Farina D. 2018 Nonlinear collisionless electron cyclotron interaction in the pre-ionisation stage *Nucl. Fusion* **58** 066012
[6] Albert Johansson C. and Aleynikov P. 2024 Electron cyclotron resonance during plasma initiation *J. Plasma Phys.* **90** 905900103
[7] Nevins W.M., Rognlien T.D. and Cohen B.I. 1987 Nonlinear absorption of intense microwave pulses *Phys. Rev. Lett.* **59** 60
[8] Neishtadt A.I. and Timofeev A.V. 1987 Autoresonance in electron cyclotron heating of a plasma *Zh. Eksp. Teor. Fiz* **93** 1706–13
[9] Farina D. and Pozzoli R. 1991 Nonlinear electron-cyclotron power absorption *Phys. Fluids* B **3** 1570–5
[10] Zvonkov A.V. and Timofeev A.V. 1986 Relativistic effects in the formation of braided electrons during cyclotron heating *Sov. J. Plasma Phys. (Engl. Transl.), (United States)* **12** 238-240L
[11] Chirikov B.V. 1960 Resonance processes in magnetic traps *J. Nucl. Energy* C **1** 253–60
[12] Eriksson L.-G. and Helander P. 2003 Simulation of runaway electrons during tokamak disruptions *Comput. Phys. Commun.* **154** 175–96
[13] Rosenbluth M.N. and Putvinski S.V. 1997 Theory for avalanche of runaway electrons in tokamaks *Nucl. Fusion* **37** 1355
[14] Breizman B.N., Aleynikov P., Hollmann E.M. and Lehnen M. 2019 Physics of runaway electrons in tokamaks *Nucl. Fusion* **59** 083001
[15] Kamikawai R., Watanabe T. and Amemiya A. 1969 Mean excitation energy for stopping power of molecular hydrogen *Phys. Rev.* **184** 303–11
[16] Shalashov A.G., Gospodchikov E.D. and Izotov. I.V. 2020 Electron-cyclotron heating and kinetic instabilities of a mirror-confined plasma: the quasilinear theory revised *Plasma Phys. Control. Fusion* **62** 065005
[17] Sunn Pedersen T. *et al* 2016 Confirmation of the topology of the Wendelstein 7-X magnetic field to better than 1: 100,000 *Nat. Commun.* **7** 13493
[18] Hoefel U., Hirsch M., Kwak S., Pavone A., Svensson J., Stange T., Hartfuß H.-J., Schilling J., Weir G. and Willem Oosterbeek J. 2019 Bayesian modeling of microwave radiometer calibration on the example of the Wendelstein 7-X electron cyclotron emission diagnostic *Rev. Sci. Instrum.* **90** 043502
[19] Hirsch M., Höfel U., Willem Oosterbeek J., Chaudhary N., Geiger J., Hartfuss H.-J., Kasparek W., Marushchenko N., van Milligen B. and Plaum B. 2019 ECE diagnostic for the initial operation of Wendelstein 7-X *EPJ Web of Conf.* (EDP Sciences) vol 203 p 03007
[20] Chaudhary N., Hirsch M., Hoefel U., Oosterbeek J.W., Marushchenko N.B., Wolf R.C. *et al* 2022 Electron temperature profile from optically grey x3-mode of electron cyclotron emission at Wendelstein 7-X using bayesian analysis *Plasma Phys. Control. Fusion* **64** 055016
[21] Brunner K.J., Akiyama T., Hirsch M., Knauer J., Kornejew P., Kursinski B., Laqua H., Meineke J., Trimiño Mora H. and Wolf R.C. 2018 Real-time dispersion interferometry for density feedback in fusion devices *J. Instrum.* **13** 09002
[22] Marushchenko N.B., Turkin Y. and Maassberg H. 2014 Ray-tracing code travis for ECR heating, EC current drive and ECE diagnostic *Comput. Phys. Commun.* **185** 165–76
[23] Northrop T.G. and Teller E. 1960 Stability of the adiabatic motion of charged particles in the earth's field *Phys. Rev.* **117** 215–25
[24] Helander P. 2014 Theory of plasma confinement in non-axisymmetric magnetic fields *Rep. Prog. Phys.* **77** 087001
[25] Beidler C.D. *et al* 2011 Benchmarking of the mono-energetic transport coefficients—results from the International Collaboration on Neoclassical Transport in Stellarators (ICNTS) *Nucl. Fusion* **51** 076001